Article

Sulfur K-Edge X-ray Absorption Spectroscopy and Density Functional Theory Calculations on Superoxide Reductase: Role of the Axial Thiolate in Reactivity

Abhishek Dey, Francis E. Jenney,, Michael W. W. Adams, Michael K. Johnson, Keith O. Hodgson, Britt Hedman, and Edward I. Solomon

J. Am. Chem. Soc., **2007**, 129 (41), 12418-12431• DOI: 10.1021/ja064167p • Publication Date (Web): 22 September 2007

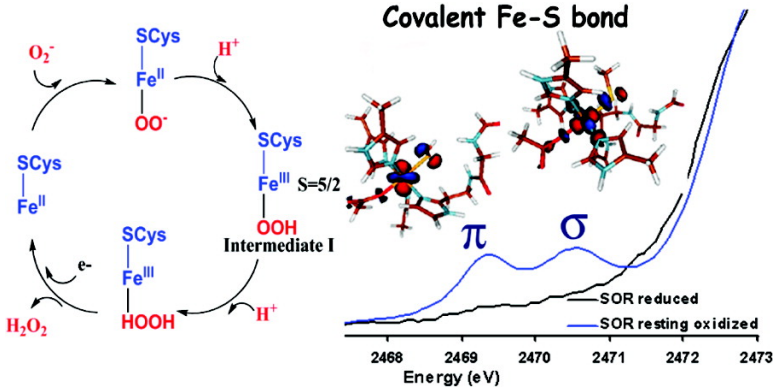

More About This Article

Additional resources and features associated with this article are available within the HTML version:

- Supporting Information
- Links to the 3 articles that cite this article, as of the time of this article download
- Access to high resolution figures
- Links to articles and content related to this article
- Copyright permission to reproduce figures and/or text from this article

View the Full Text HTML

J|A|C|S
ARTICLES
Published on Web 09/22/2007

Sulfur K-Edge X-ray Absorption Spectroscopy and Density Functional Theory Calculations on Superoxide Reductase: Role of the Axial Thiolate in Reactivity

Abhishek Dey,[†] Francis E. Jenney, Jr.,[§] Michael W. W. Adams,[§] Michael K. Johnson,[§] Keith O. Hodgson,*[,†,‡] Britt Hedman,*[,‡] and Edward I. Solomon*[,†,‡]

Contribution from the Department of Chemistry, Stanford University, Stanford, California 94305, Departments of Chemistry and Biochemistry & Molecular Biology, University of Georgia, Athens, Georgia 30602, and Stanford Synchrotron Radiation Laboratory, SLAC, Stanford University, Menlo Park, California 94025

Received June 13, 2006; E-mail: edward.solomon@stanford.edu

Abstract: Superoxide reductase (SOR) is a non-heme iron enzyme that reduces superoxide to peroxide at a diffusion-controlled rate. Sulfur K-edge X-ray absorption spectroscopy (XAS) is used to investigate the ground-state electronic structure of the resting high-spin and CN^- bound low-spin Fe^{III} forms of the 1Fe SOR from *Pyrococcus furiosus*. A computational model with constrained imidazole rings (necessary for reproducing spin states), H-bonding interaction to the thiolate (necessary for reproducing Fe−S bond covalency of the high-spin and low-spin forms), and H-bonding to the exchangeable axial ligand (necessary to reproduce the ground state of the low-spin form) was developed and then used to investigate the enzymatic reaction mechanism. Reaction of the resting ferrous site with superoxide and protonation leading to a high-spin Fe^{III}−OOH species and its subsequent protonation resulting in H_2O_2 release is calculated to be the most energetically favorable reaction pathway. Our results suggest that the thiolate acts as a covalent anionic ligand. Replacing the thiolate with a neutral noncovalent ligand makes protonation very endothermic and greatly raises the reduction potential. The covalent nature of the thiolate weakens the Fe^{III} bond to the proximal oxygen of this hydroperoxo species, which raises its pK_a by an additional 5 log units relative to the pK_a of a primarily anionic ligand, facilitating its protonation. A comparison with cytochrome P450 indicates that the stronger equatorial ligand field from the porphyrin results in a low-spin Fe^{III}−OOH species that would not be capable of efficient H_2O_2 release due to a spin-crossing barrier associated with formation of a high-spin 5C Fe^{III} product. Additionally, the presence of the dianionic porphyrin π ring in cytochrome P450 allows O−O heterolysis, forming an Fe^{IV}−oxo porphyrin radical species, which is calculated to be extremely unfavorable for the non-heme SOR ligand environment. Finally, the 5C Fe^{III} site that results from the product release at the end of the O_2^- reduction cycle is calculated to be *capable* of reacting with a second O_2^-, resulting in superoxide dismutase (SOD) activity. However, in contrast to FeSOD, the 5C Fe^{III} site of SOR, which is more positively charged, is calculated to have a high affinity for binding a sixth anionic ligand, which would inhibit its SOD activity.

Introduction

The enzyme superoxide reductase (SOR) is found in microaerophilic and strictly anaerobic microorganisms and is capable of reducing superoxide to peroxide.[1−5] Though its *in vivo* function is not completely understood, it is thought to provide a mechanism for combating oxidative stress in anaerobes, which typically lack the classical superoxide dismutases (SOD), by depleting superoxide concentration via direct reduction to hydrogen peroxide, rather than by a dismutation reaction which produces H_2O_2 and O_2.[6] Thus, unlike SOD, SOR does not accumulate dioxygen in these highly anoxic microorganisms. The crystal structure of the resting oxidized form of the 1Fe-SOR from *Pyrococcus furiosus* (Figure 1) shows that the ferric active site has a non-heme iron coordinated to four histidines in the equatorial plane and a cysteine and glutamate in the transaxial positions.[7] There are two peptide N−H---SCys H-bonds to the axial cysteine ligand. Both 1Fe and 2Fe SORs have been characterized and found to have similar active-site structures and reactivities.[8,9] The second Fe in the 2Fe SOR is in a

[†] Department of Chemistry, Stanford University.
[§] University of Georgia.
[‡] Stanford Synchrotron Radiation Laboratory.

(1) Jenney, F. E., Jr.; Verhagen, M. F. J. M.; Cui, X.; Adams, M. W. W. *Science* **1999**, *286*, 306−309.
(2) Kurtz, D. M., Jr.; Coulter, E. D. *J. Biol. Inorg. Chem.* **2002**, *7*, 653−658.
(3) Adams, M. W. W.; Jenney, F. E., Jr.; Clay, M. D.; Johnson, M. K. *J. Biol. Inorg. Chem.* **2002**, *7*, 647−652.
(4) Nivière, V.; Fontecave, M. *J. Biol. Inorg. Chem.* **2004**, *9*, 119−123.
(5) Abreu, I. A.; Xavier, A. V.; LeGall, J.; Cabelli, D. E.; Teixeira, M. *J. Biol. Inorg. Chem.* **2002**, *7*, 668−674.
(6) Imlay, J. A. *J. Biol. Inorg. Chem.* **2002**, *7*, 659−663.
(7) Yeh, A. P.; Hu, Y.; Jenney, F. E., Jr.; Adams, M. W.; Rees, D. C. *Biochemistry* **2000**, *39*, 2499−2508.

10.1021/ja064167p CCC: $37.00

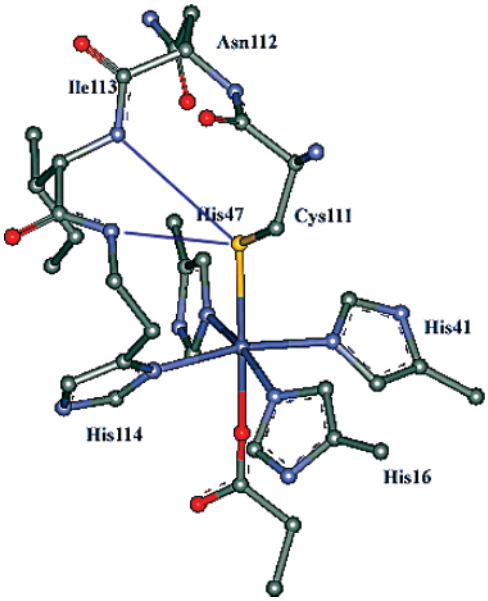

Figure 1. Active site of SOR from *P. furiosus* at 1.7 Å resolution (PDB: 1DQI).[7] Residues Ile113 and Asn112 are in the vicinity of the active site and proposed to H-bond to the Cys111 thiolate.

rubredoxin-like $Fe(SCys)_4$ site, for which the function is unknown, as eliminating it by mutation does not affect the reactivity of this enzyme.[9]

The resting oxidized form of 1Fe *P. furiosus* SOR has been spectroscopically characterized in detail by Clay et al.[10,11] It has a high-spin ground state and an intense $CysS^- \rightarrow Fe^{III}$ charge-transfer (CT) band at 15 100 cm^{-1} ($\epsilon \approx 2500\ M^{-1}\ cm^{-1}$), which gives it its characteristic blue color. The EPR spectrum of the high-spin resting state indicated that it is quite axial ($E/D = 0.06$), and variable-temperature, variable-pressure magnetic circular dichroism (VTVH MCD) indicated that a trans $N_{His}-Fe-N_{His}$ axis defined the unique direction of the zero-field splitting tensor and not the trans $S_{Cys}-Fe-O_{Glu}$ axis.[10] This site is solvent-exposed and binds exogenous ligands such as N_3^- and OH^- in place of the glutamate. Binding CN^- converts it to a low-spin site with an intense $CysS^- \rightarrow Fe^{III}$ CT at 14 600 cm^{-1} ($\epsilon \approx 2700\ M^{-1}\ cm^{-1}$).[10]

The reaction mechanism of SOR, involving transfer of an electron and two protons to superoxide to form hydrogen peroxide, has been studied in detail using kinetic and spectroscopic techniques.[12−18] Using kinetic data, Nivière et al. and Kurtz et al. have proposed the presence of at least one Fe^{III} intermediate (henceforth referred to as intermediate I, characterized by a CT band at 600 nm) in the reaction. The formation of the intermediate is diffusion controlled and has no pH dependence or deuterium isotope effect and thus is proposed to be an $Fe^{III}-\mu_2\text{-}O_2^{2-}$ species. The decay of this intermediate involved a diffusion-controlled protonation, deduced from its pH dependence and a deuterium isotope effect of 2. Lys14 has been identified as a participating second-sphere residue (mutation of this residue decreases the turnover rate by a factor of 20−30) and has been proposed to assist superoxide binding to the active site.[19,20] Though no intermediate has been trapped with the physiological substrate superoxide, Olivier et al. have trapped and characterized [using electron paramagnetic resonance (EPR), resonance Raman (rRaman), and Mössbauer spectroscopies and density functional theory (DFT) calculations] a high-spin ($S = {}^5/_2$) side-on $\eta^2\text{-}O_2^{2-}-Fe^{III}$ species by addition of H_2O_2 to the resting Fe^{II} form of the enzyme.[21,22] The relevance of such species in the turnover cycle of SOR is still an open issue.[23]

A computational study has used DFT to investigate the ground state and has considered possible intermediates along the reaction pathway.[17] The study successfully reproduced most of the geometric parameters and spin state of the experimentally observed high-spin ferrous and ferric ground states and concluded that a low-spin $Fe^{III}-OOH$ is the best candidate for the intermediate I. A subsequent protonation-driven H_2O_2 release from this low-spin $Fe^{III}-OOH$ was proposed, though the energetic feasibility of such steps was not evaluated.[17] Kovacs et al.[24] reported a high-spin intermediate, and Kovacs et al.[25] and Goldberg et al.[26] reported low-spin $Fe^{III}-OOH(R)$ intermediates, upon reacting Fe^{II} SOR model complexes with superoxide or alkyl peroxide in protic solvents. The former study reported weak Fe−O and high O−O stretches in the rRaman spectrum which correlated with the facile rate of dissociation of H_2O_2 from the $Fe^{III}-OOH$ intermediate in presence of weak acids, e.g., methanol.[24]

The presence of an axial cysteine ligand distinguishes the SOR active site from all other catalytic non-heme Fe enzymes. The role of this thiolate ligand is currently an open issue. The weak Fe−O bond in the high-spin $Fe^{III}-OOH$ model studied by Kovacs et al. requires a strong trans effect of the axial thiolate.[24] The trans effect of the thiolate has also been proposed to affect NO binding to this active site.[27] The thiolate may also play a major role in controlling the reduction potential of the active site.[23] Alternatively, there is some similarity between the SOR active site and the active site of cytochrome P450, where the four porphyrin nitrogens are in the equatorial plane and there

(8) Coehlo, A. V.; Matias, P.; Fülop, V.; Thomson, A.; Gonzalez, A.; Carrondo, M. A. *J. Biol. Inorg. Chem.* **1997**, *2*, 680−689.
(9) Emerson, J. P.; Cabelli, D. E.; Kurtz, D. M., Jr. *Proc. Natl. Acad. Sci. U.S.A.* **2003**, *100*, 3802−3807.
(10) Clay, M. D.; Jenney, F. E., Jr.; Hagedoorn, P. L.; George, G. N.; Adams, M. W. W.; Johnson, M. K. *J. Am. Chem. Soc.* **2002**, *124*, 788−805.
(11) Clay, M. D.; Jenney, F. E., Jr.; Noh, H. J.; Hagedoorn, P. L.; Adams, M. W W.; Johnson, M. K. *Biochemistry* **2002**, *41*, 9833−9841.
(12) Coulter, E. D.; Emerson, J. P.; Kurtz, D. M., Jr.; Cabelli, D. E. *J. Am. Chem. Soc.* **2000**, *122*, 11555−11556.
(13) Nivière, V.; Lombard, M.; Fontecave, M.; Houée-Levin, C. *FEBS Lett.* **2001**, *497*, 171−173.
(14) Emerson, J. P.; Coulter, E. D.; Cabelli, D. E.; Phillips, R. S.; Kurtz, D. M., Jr. *Biochemistry* **2002**, *41*, 4348−4357.
(15) Nivière, V.; Asso, M.; Weill, C. O.; Lombard, M.; Guigliarelli, B.; Favaudon, V.; Houée-Levin, C. *Biochemistry* **2004**, *43*, 808−818.
(16) Lombard, M.; Touati, D.; Fontecave, M.; and Nivière, V. *J. Biol. Chem.* **2000**, *275*, 27021−27026.
(17) Silaghi-Dumitrescu, R.; Silaghi-Dumitrescu, I.; Coulter, E. D.; Kurtz, D. M., Jr. *Inorg. Chem.* **2003**, *42*, 446−456.
(18) Halfen, J. A.; Moore, H. L.; Fox, D. C. *Inorg. Chem.* **2002**, *41*, 3935−3943.
(19) Lombard, M.; Houée-Levin, C.; Touati, D.; Fontecave, M.; Nivière, V. *Biochemistry* **2001**, *40*, 5032−5040.
(20) Clay, M. D.; Yang, T.-C.; Jenney, F. E., Jr.; Kung, I. Y.; Cosper, C. A.; Krishnan, R.; Kurtz, D. M., Jr.; Adams, M. W. W.; Hoffman, B. M.; Johnson, M. K. *Biochemistry* **2006**, *45*, 427−438.
(21) Mathé, C.; Mattioli, T. A.; Horner, O.; Lombard, M.; Latour, J.-M.; Fontecave, M.; Nivière, V. *J. Am. Chem. Soc.* **2002**, *124*, 4966−4967.
(22) Horner, O.; Mouesca, J. M.; Oddou, J. L.; Jeandey, C.; Nivière, V.; Mattioli, T. A.; Mathé, C.; Fontecave, M.; Maldivi, P.; Bonville, P.; Halfen, J. A.; Latour, J. M. *Biochemistry* **2004**, *43*, 8815−8825.
(23) Kurtz, D. A. *Acc. Chem. Res.* **2004**, 37, 902−908.
(24) Kitagawa, T.; Dey, A.; Lugo-Mas, P.; Solomon, E. I.; Kovacs, J. A *J. Am. Chem. Soc.* **2006**, *128*, 14448−14449.
(25) Shearer, J.; Scarrow, R. C.; Kovacs, J. A. *J. Am. Chem. Soc.* **2002**, *124*, 11709−11717.
(26) Krishnamurthy, D.; Kasper, G. D.; Namuswe, F.; Kerber, W. D.; Narducci Sarjeant, A. A.; Moenne-Loccoz, P.; Goldberg, D. P. *J. Am. Chem. Soc.* **2006**, *128*, 14222−14223.
(27) Clay, M. D.; Cosper, C. A.; Jenney, F. E.; Adams, M .W. W.; Johnson, M. K. *Proc. Natl. Acad. Sci. U.S.A.* **2003**, *100*, 3796−3801.

is an axial cysteine ligand.[28] However, these sites differ drastically in reactivity. SOR releases hydrogen peroxide via proton-assisted heterolytic cleavage of the Fe−O bond, and P450 activates O_2 to oxidize substrates via a low-spin Fe^{III}−OOH intermediate which protonates at the distal oxygen to heterolytically cleave the O−O bond to form compound I.[29,30] Also, despite having a favorable redox potential (+250 mV), the SOR active site is incapable of exhibiting SOD activity.[31] The reduced SOR (Fe^{II} form) will reduce O_2^- to H_2O_2, but the oxidized SOR (Fe^{III} form) will not oxidize O_2^- to O_2.[23] This is crucial in maintaining low oxidative stress in anaerobes that are proposed to use SOR to deplete the superoxide concentration *in vivo*. However, FeSOD, with nitrogen- and oxygen-based ligands, can perform both reactions. The lack of an open coordination site has been suggested to be a possible reason for this,[23] although the origin of the affinity for this sixth ligand binding or the feasibility of a SOD reaction in a SOR active site has not been evaluated. Thus, it is important to understand the role of the axial thiolate ligand and the lack of heme in determining the reactivity of SOR.

Sulfur K-edge X-ray absorption spectroscopy (S K-edge XAS) is a relatively new spectroscopic method that has been used to study metal−sulfur (M−S) bonding and how it is affected by the protein in various Cu−S and Fe−S electron-transfer (ET) active sites.[32−34] The S K-edge refers to the ionization of the sulfur 1s (S_{1s}) orbital. This is a ligand-based transition, and thus this technique does not suffer from the complications that arise from the interaction of the core hole with the metal 3d manifold in the final state.[35] The, lower-energy pre-edge transitions to unoccupied metal 3d (M_{3d}) orbitals gain intensity through sulfur 3p (S_{3p}) mixing due to covalency and because the sulfur 1s → 3p transition is electric-dipole-allowed. Thus, the S K-pre-edge intensity is a direct experimental probe of M−S bond covalency. Recently, we have used this method to investigate the active-site structure and bonding in a series of P450 model complexes to quantitatively understand the effect of H-bonding on Fe−thiolate bond covalency and redox potential.[36]

In the present study, we use S K-edge XAS to quantitatively define the Fe−S bond covalency in the resting high-spin and CN^--bound low-spin ferric forms of SOR from *P. furiosus*. We use the S K-edge results in addition to other well-defined experimental parameters, e.g., geometry, spin states, Fe−S bond covalency, etc., to develop a computational model for the resting ferric SOR active site that required inclusion of H-bonding to the axial thiolate ligand. The S K-edge XAS data on the low-spin CN^- bound form are then used to evaluate computational models for this spin state change and further expand the model to include H-bonding to the exchangeable axial ligand. The model that best fits these experimental data is then used to computationally investigate the proposed mechanism of SOR and evaluate possible intermediates. The role of the trans axial thiolate and H-bonding to it in the SOR reaction are computationally evaluated. The Fe^{III}−OOH species in the SOR site is compared to that in P450 (compound 0). The role of the non-heme vs heme ligand in the difference in their reactivities is evaluated. A hypothetical SOD reaction cycle is constructed for the SOR active site and compared to that for the Fe−SOD active site to obtain insight into the lack of SOD reactivity of SOR.

Experimental Details

Sample Preparation. The recombinant form of *P. furiosus* SOR was obtained from *Escherichia coli* as described in ref 10. Absorption at 660 nm (ϵ = 2500 M^{-1} cm^{-1})[10] indicated that 85% of the protein was loaded with Fe. The protein solutions (in 100 mM phosphate buffer having pH 7.2−7.3) were pre-equilibrated in a water-saturated He atmosphere for ∼1 h to minimize bubble formation in the sample cell. The protein samples were oxidized or reduced before experiments by using a ∼3−4-fold excess of sodium hexachloroiridate or ascorbic acid solution in the same buffer as the protein solution. The CN^- bound form was generated by adding 40 equiv of CN^- to a pre-oxidized sample at pH 9.0. The complete conversion to the low-spin form was confirmed by room-temperature absorption and EPR spectroscopy at 8 K (Figure S1, Supporting Information). Samples were loaded via a syringe into a Pt-plated Al block sample holder, sealed in front using a 6.3 μm polypropylene window and maintained at a constant temperature of 4 °C during data collection using a controlled flow of N_2 gas, pre-cooled by liquid N_2 passing through an internal channel in the Al block.

Data Collection and Reduction. XAS data were measured at the Stanford Synchrotron Radiation Laboratory using the 54-pole wiggler beam line 6-2. Details of the experimental configuration for low-energy studies have been described previously.[37] The energy calibration, data reduction, and error analysis follow the same approach described previously.[38]

Fitting Procedures. Pre-edge features were fit using pseudo-Voigt line shapes (sums of Lorentzian and Gaussian functions) using the program PEAKFIT. This line shape is appropriate as the experimental features are expected to be a convolution of a Lorentzian transition envelope[39] and a Gaussian line shape imposed by the beam line optics.[40] A fixed 1:1 ratio of Lorentzian to Gaussian contribution successfully reproduced the pre-edge features. The rising edges were also fit with pseudo-Voigt line shapes. Fitting requirements included reproducing the data *and* its second derivative, using a minimum number of peaks. Fits were performed using single peaks to simulate the pre-edge feature of each component with a half-width of ∼0.9 eV. The intensity of a pre-edge feature (peak area) represents the sum of the intensity of all the pseudo-Voigt peaks which were needed to fit the feature in a given fit. The fitted intensities were converted to $\%S_{3p}$ character using the pre-edge feature of plastocyanin as a reference (where 1.27 units of intensity, obtained using this program, corresponded to 38% S_{3p} character).[41] Note that the 85% loading of the active site was accounted

(28) Poulos, T. L.; Finzel, B. C.; Howard, A. J. *J. Mol. Biol.* **1987**, *195*, 687−700.
(29) Meunier, B.; de Visser, S. P.; Shaik, S. *Chem. Rev.* **2004**, *104*, 3947−3980.
(30) Akhtar, M.; Calder, M. R.; Corina, D. L.; Wright, J. N. *Biochem. J.* **1982**, *201*, 569−580.
(31) Jovanović, T.; Ascenso, C.; Hazlett, K. R. O.; Sikkink, R.; Krebs, C.; Litwiller, L. M.; Benson, L. M.; Moura, I.; Moura, J. J. G.; Radolf, J. D.; Huynh, B. H.; Naylor, S.; Rusnak, F. M. *J. Biol. Chem.* **2000**, *275*, 28439−28448.
(32) Solomon, E. I.; Hedman, B.; Hodgson, K. O.; Dey, A.; Szilagyi, R. K. *Coord. Chem. Rev.* **2005**, *249*, 97−129.
(33) Dey, A.; Glaser, T.; Moura, J. J. G.; Holm, R. H.; Hedman, B.; Hodgson, K. O.; Solomon, E. I. *J. Am. Chem. Soc.* **2004**, *126*, 16868−16878.
(34) Solomon, E. I.; Gorelsky, S. I.; Dey, A. *J. Comput. Chem.* **2006**, *27*, 1414−1428.
(35) Neese, F.; Hedman, B.; Hodgson, K. O.; Solomon, E. I. *Inorg. Chem.* **1999**, *38*, 4854−4860.
(36) Dey, A.; Okamura, T.-A.; Ueyama, N.; Hedman, B.; Hodgson, K. O.; Solomon, E. I. *J. Am. Chem. Soc.* **2005**, *127*, 12046−12053.
(37) Hedman, B.; Frank, P.; Gheller, S. F.; Roe, A. L.; Newton, W. E.; Hodgson, K. O. *J. Am. Chem. Soc.* **1988**, *110*, 3798−3805.
(38) Shadle, S. E.; Hedman, B.; Hodgson, K. O.; Solomon, E. I. *Inorg. Chem.* **1994**, *33*, 4235−4244.
(39) Agarwal, B. K. *X-ray Spectroscopy*; Springer-Verlag: Berlin, 1979; pp 276 ff.
(40) Tyson, T. A.; Roe, A. L.; Frank, P.; Hodgson, K. O.; Hedman, B. *Phys. Rev. B* **1989**, *39A*, 6305−6315.

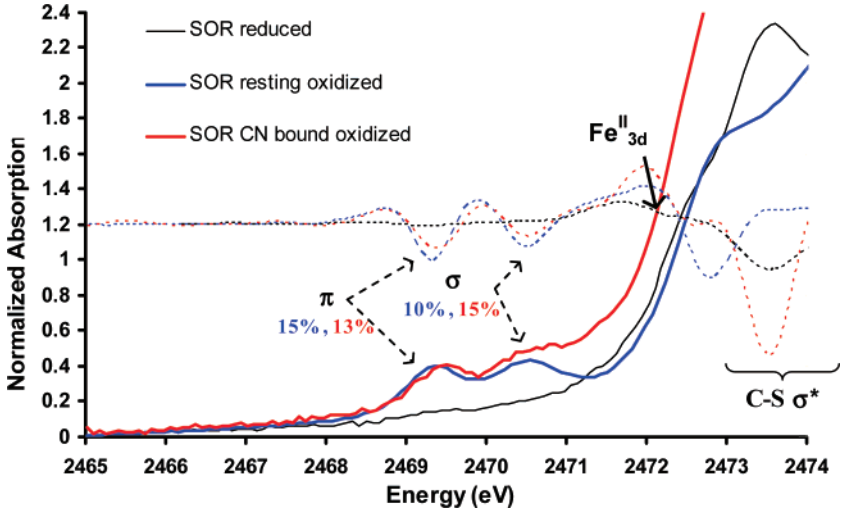

Figure 2. S K-edge XAS of superoxide reductase in its reduced (black), resting oxidized (blue), and CN^- bound oxidized (red) forms. The second derivatives of the data are shown in dotted lines. The Fe^{II} pre-edge feature is indicated by the black arrow.

for by renormalization of the data. This is because the free cysteines that are not bound to iron will contribute to the rising edge but not to the pre-edge.

DFT Calculations. All calculations were performed on dual Intel Xeon workstations using ADF 2004.01 and the Gaussian 03 package.[42] The different computational models used in this study are described and evaluated in the Results section. The geometries were optimized using either (a) the meta GGA BP86 functional available in the ADF package using a TZP basis set on all atoms or (b) the B3LYP method with 6-311G* basis sets on Fe, S, N, and O atoms and 6-31G* basis set on C and H atoms using the Gaussian 03 program.[43] The default convergence criteria in both software packages were used during optimization. For the Gaussian-optimized geometries, the energies were obtained from single-point calculations using the 6-311G* basis set on all atoms. The stability of the ground states was tested using the "stable" command in the Gaussian program. Frequency calculations were performed on the optimized geometries to ensure that they had no imaginary mode. Only the larger H-bonded models having seven frozen coordinates had four or five <30 cm^{-1} imaginary modes involving these frozen coordinates. For calculating the SOD reaction, the coordinates from the X-tal structure of Fe−SOD from *Propionibacterium shermanii* (PDB ID: 1BSM) were used for the starting structure.[44] The α-carbons of the histidine and the glutamate residues were frozen during optimization. All other geometric parameters were optimized. Mulliken[45] population analyses were performed using the PYMOLYZE program,[46] and the molecular orbitals were plotted using Molden version 4.1 with a contour value of 0.05. For solvent corrections, experimental free energies of solvation were used for all small ions (since the site is solvent exposed), and a polarizable continuum model (PCM)[47] with an ϵ of 4.0 was applied to the active-site models.[48] The fragment dissociation energies (bond energies) were computed by comparing the energies of the full molecule to the sum of the energies of the fragments. To check for basis set superposition error, we estimated the energies of the two weakly endothermic key protonation steps with a larger 6-311+g** basis set and found less than 2 kcal difference in the calculated energies.

Results

A. S K-Edge XAS. The S K-edge XAS data for the resting oxidized (blue), CN^- bound oxidized (red), and reduced (black) forms of SOR enzymes are shown in Figure 2. The XAS data of the resting oxidized species show two distinct pre-edge features at 2469.3 and 2470.5 eV and a rising edge transition at 2472.8 eV. The two pre-edge features correspond to S_{1s} transitions to the t_2 and e half-occupied molecular orbitals of the resting high-spin ferric ground state. These features can be quantified by fits to the experimental data to have 0.49 and 0.33 unit of normalized intensity, respectively. These correspond to 15 ± 2% and 10 ± 2% S_{3p} character in the singly occupied d-π (t_2) and the d-σ (e) orbitals, respectively, in the d^5 resting oxidized high-spin ground state. The CN^- bound low-spin form (Figure 2, red) also exhibits t_2 and e transitions at 2469.5 and 2470.7 eV, with 0.50 and 0.48 unit of intensity, respectively.[49] These correspond to 13 ± 2% and 15 ± 3% S_{3p} character mixed into the singly occupied t_2 π and unoccupied e σ orbitals, respectively, of the low-spin d^5 ferric state. The significant intensity in the low-energy peak indicates that the single d-π t_2 hole is oriented along the Fe−S bond. Although one may have expected the e intensity to go up in the low-spin form (as both α and β Fe−S d-σ orbitals are unoccupied in the low-spin state relative to one β d-σ orbital in the high-spin state and the Fe−S bond length is shorter), the intensity actually goes down. However, for low-spin Fe^{III}, the assignment of the pre-edge features is complicated by multiplet effects in the final state. The $S_{1s} \rightarrow Fe_{3d}$ transition produces an $\underline{L}^1t_2^5e^1$ excited-state configuration (where $\underline{L}$ = ligand hole), which produces two ^2A excited states (the $t_2^5e^1$ configuration produces a singlet and triplet state which couple to the ligand hole). These wave functions were obtained as linear combinations of the parent microstates using lowering operators.[50,51] The ^2A state origi-

(41) Shadle, S. E.; Penner-Hahn, J. E.; Schugar, H. J.; Hedman, B.; Hodgson, K. O.; Solomon, E. I. *J. Am. Chem. Soc.* **1993**, *115*, 767−776.
(42) Frisch, M. J.; et. al. *Gaussian 03*, Revision C 02; Gaussian, Inc.: Wallingford, CT, 2004.
(43) Becke, A. D. *J. Chem. Phys.* **1993**, *98*, 5648−5652.
(44) Schmidt, M. *Eur. J. Biochem.* **1999**, *262*, 117−127.
(45) Mulliken, R. S. J. *Chem. Phys.* **1955**, *23*, 1833−1840.
(46) Tenderholt, A. L. *PyMOlyze*, Version 1.1; Stanford University, Stanford, CA, 2006 (http://pymolyze.sourceforge.net).
(47) Miertus, S.; Scrocco, E.; Tomasi, J. *Chem. Phys.* **1981**, *55*, 117−129.
(48) Gogonea, V.; Merz, M. K., Jr. *J. Phys. Chem. A* **1999**, *103*, 5171−5188.
(49) Note that the higher energy feature is hard to estimate, as it strongly overlaps with the very strong $S_{1S} \rightarrow C-S\sigma^*$ transition.
(50) Van Vleck, J. H. *Phys. Rev.* **1934**, 45, 405.
(51) Laporte, O. *Phys. Rev.* **1942**, 61, 302−304.

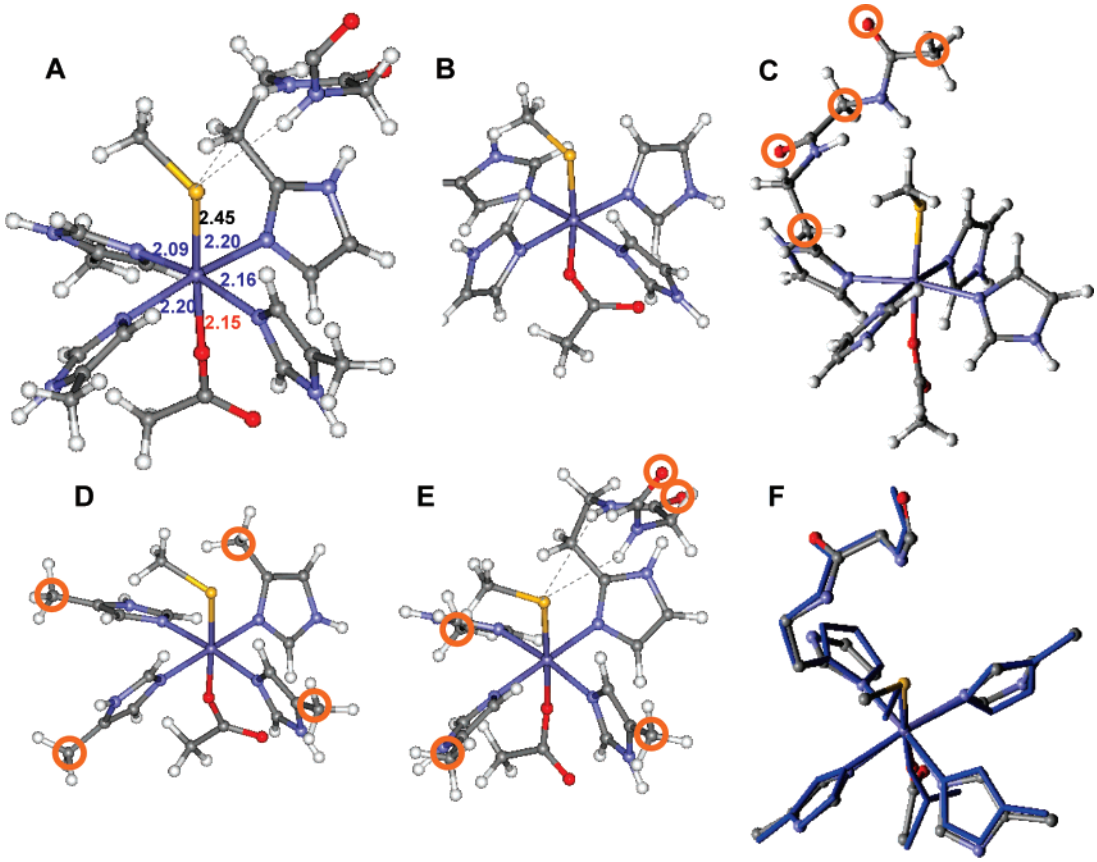

Figure 3. Crystal structure of the active site of resting oxidized SOR (A), the unconstrained model (B), H-bonded only model (C),[60] α-carbon constrained model (D), H-bonded and α-carbon constrained model (E), and overlay between the optimized model E (in blue) and X-tal structure (atom colored) from 1DQI (F). The constrained atoms are circled in the respective structures. Bond lengths of the protein crystal structure are given in angstroms and are color coded as follows: Fe−S, black; Fe−N, blue; and Fe−O, red.

nating from the parent d^{n+1} triplet configuration has 3 times the intensity of the ^2A state originating from the d^{n+1} singlet parent configuration. The observed pre-edge feature at 2470.5 eV can be assigned as the transition to the lower ^2A state (originating from the triplet d^{n+1} parent) with $^3/_4$ of the intensity, while the higher energy multiplet should be shifted up in energy (estimated ∼1 eV from DFT)[52] and obscured by overlap with the C−S σ^* transition.[53] Corrected for this multiplet shift of intensity, the total intensity for the e transition in the low-spin state is 20%.

The data for the resting reduced form show an intense $S_{1s} \rightarrow S_{C-S\ \sigma^*}$ transition at 2473.6 eV. The $S_{1s} \rightarrow Fe^{II}{}_{3d}$ pre-edge transition appears as a weak feature in the second derivative of the data[54] at 2472.1 eV (Figure 2, arrow on dotted black line), overlapping with the stronger feature at 2473.6 eV.

B. DFT Modeling. 1. High-Spin Resting. The active site was modeled using the crystal structure of 1Fe SOR (PDB: 1DQI)[7] with four neutral imidazole rings (representing the coordinated histidines), an axial methyl thiolate (representing cysteine), and an axial acetate (representing glutamate) (Figure 3A). Geometry-optimized DFT calculations were performed using BP86 and B3LYP methods on four sets of models (B, C, D, and E), presented in Figure 3. The relevant optimized parameters are given in Table 1. Full optimization of the active site using BP86 with no constraints led to structure B (Figure 3), where the metal−ligand bond lengths were in good agreement with the published solution EXAFS results (Figure 3A) and the 1.7 Å resolution crystal structure.[7,10] However, the optimized low-spin state was found to be more stable by 11.2 kcal/mol (Table 1). This indicates that the full optimization, which does not include the constraints imposed by the protein environment, does not correctly describe the ground state at the BP86 level. This could be either a result of the simplified model that does not account for the constraints imposed on an active site by the protein backbone or an artifact of using a pure density functional, which generally stabilizes a low-spin state.[55]

Two conserved H-bonds to the axial $CysS^-$ (see Figure 1) from the amide N−H's of the His114 and Ile113 residues are present in the active site of SOR that are absent in model B. These H-bonds can affect the covalency of the axial Fe−S bond and may be an important determinant of the spin state. Thus, the two H-bonds were also included in the model and optimized (the carbonyl oxygens of the H-bonding amides were frozen in space during optimization, as these are strongly H-bonded to second-sphere residues, see Figure 3C). The optimized bond lengths and bond angles of the high-spin (HS) and low-spin(LS) states are given in Table 1. The H-bonding to CysS causes

(52) The energy splitting between these triplet and broken-symmetry singlet d^{n+1} states was evaluated from DFT calculations to be 0.45 eV. From spin projection, the T/S splitting is twice this value, i.e., 0.9 eV.
(53) Note that there is a weak shoulder in the data in Figure 2 (red) at 2471.5 eV (∼1 eV above the e feature) that is also visible in the second derivative of the spectra (dashed red). However, due to its overlap with the intense rising edge feature, it could not be quantified.
(54) A minimum in second derivative indicates a maximum in absorption.
(55) Note that, in ref 17, a high-spin ground state was obtained using BP86 and a double-ζ basis set. Using Gaussian 03 and ADF, we found the low-spin ground state to be more stable using the BP86 functional, irrespective of the quality of the basis set used.

Table 1. Geometric Parameters and Energy Difference of Models B, C, D, and E, Calculated Using BP86 and B3LYP Methods

method	model	Fe–S[a]	Fe–N_1[a,b]	Fe–N_2[a,b]	Fe–O[a]	C–S–Fe[c]	N–S[a]	S---H–N[c]	ΔE_{HS-LS}[d]
X-ray	1DQI	2.46	2.12	2.20	2.15	117.0	3.50, 3.72	131.7, 165.1	
EXAFS		2.36	2.17	2.07	2.15				
BP86	B-HS	2.39	2.18	2.22	2.03	111.5			+11.2
	B-LS	2.21	2.00	2.03	2.03	113.0			
	C-HS	2.42	2.20	2.22	1.97	121.4	3.62, 3.82	112.8, 140.9	+9.0
	C-LS	2.20	2.01	2.02	1.98	114.7	3.69, 3.97	107.2, 137.1	
	D-HS	2.39	2.15	2.20	2.03	120.1			+4.5
	D-LS	2.23	2.05	2.06	2.00	124.4			
B3LYP	D-HS	2.43	2.18	2.18	2.01	109.9			−20.0
	D-LS	2.31	2.02	2.03	1.98	109.6			
	E-HS	2.43	2.15	2.20	1.95	111.4	3.65, 3.90	126.0, 144.5	−6.8
	E-LS	2.28	2.07	2.04	1.97	113.0	3.81, 4.03	121.8, 143.6	

[a] In angstroms. [b] The Fe−N distances are grouped together, representing long and short Fe−N bonds. [c] In degrees. [d] In kilocalories per mole.

∼0.03 Å elongation of the Fe−S bond length in the optimized structures for both spin sates. Also, the H-bonding interaction is weaker in the low-spin state, as indicated by the longer N−S heteroatom distances and less linear N−H−S angles (Table 1). This is because the Fe−S bond is more covalent in the low-spin state, which shifts electron density away from the thiolate and weakens the H-bonding interaction. Note that, even in this model, the optimized structure of the low-spin state shows significant shortening of the Fe−N_{His} bond length relative to that in the high-spin state (like in model B), and this results in a 9 kcal/mol more stable low-spin state. This implies that, though the H-bonding weakens the Fe−S bond, it does not result in a high-spin ground state for this model of SOR.

In the crystal structure of the enzyme, the coordinated histidine residues are involved in direct or indirect (via bridging water molecules) H-bonds from peptide residues (e.g., pro42). These H-bonding interactions will oppose the shortening of Fe−N_{His} bond lengths observed in these unconstrained calculations that may lead to a low-spin ground state. To simulate this tethering of the histidine residues, the active-site model was expanded to include the α-carbon of the four histidine rings that were frozen during optimization (Figure 3D). Though the resulting geometry is generally in good agreement with the solution EXAFS results (Table 1), the low-spin ground state is still more stable, albeit the energy difference between the spin states in this model is only 5 kcal/mol, relative to 11.2 kcal/mol in the unconstrained model without the H-bond (Figure 3B).[56,57]

DFT calculations were performed on model C using the hybrid B3LYP method, which is reportedly less covalent than a pure functional and thus favors the high-spin state.[58] In this α-carbon constrained model (Figure 3C), the optimized high-spin ground state is more stable than the optimized low-spin ground state by 20 kcal/mol, thus reproducing the experimentally observed high-spin ground state of a resting six-coordinate SOR active site.[59] The optimized Fe−S distances in B3LYP are ∼0.04 Å longer than those obtained from BP86 calculations. This is a consequence of overestimation of Fe−S bond covalency by a pure functional.[58] However, this model does not reproduce one short N−Fe−N (Fe−N_{His}, 2.09 and 2.16 Å) and one long N−Fe−N (Fe−N_{His}, 2.20 and 2.20 Å) axis, as observed in the active site structure. Though this geometric feature may not contribute to reactivity, it serves as another parameter to test the accuracy of these calculations.[10] As a final step, we included the H-bonding (which affected the Fe−S bond length) and the α-carbon constraints on the histidines (which affected the spin state) in the same model (Figure 3E). This B3LYP-optimized structure reproduces the experimental Fe−S bond length and has one short N_1−Fe−N_1 axis (Fe−N_1, 2.17 and 2.14 Å) and one long N_2−Fe−N_2 axis (Fe−N_2, 2.20 and 2.19 Å), and the high-spin state is 6.8 kcal/mol more stable. Note that the H-bonding residue is covalently linked to one of the histidine ligands with the longer Fe−N_{His} bond (Figure 3E). This suggests that this Fe−N_{His} bond elongation may be a result of steric interaction between the H-bonding arm and the histidine imidazole ring. We considered the possibility of a H_2O molecule H-bonded to the Glu residue, since the active site is solvent-exposed (Table 1) and there is direct Raman evidence for a solvent interaction in the low-spin CN^- form (*vide infra*). However, no significant change in geometry was observed, other than a ∼0.04 Å elongation of the Fe−O Glu bond upon H-bonding.

2. Electronic Structure. The MO diagrams (spin-unrestricted unoccupied β orbitals from the B3LYP calculations) of the resting six-coordinate ferric site without (left) and with (right) H-bonding show a pseudo-octahedral ligand field (Figure 4, left). In both models, there are two Fe−S bonding interactions. The lower energy t_2 orbital forms a π bond with the out-of-C−S−Fe plane $CysS_{3p}$ orbital, while the highest energy e orbital has a pseudo-σ interaction with the in-plane S_{3p} orbital (Figure 4, Fe−S π and Fe−S σ).[61] In the non-H-bonded models, these $\%S_{3p}$ covalencies are calculated to be 28% (π) and 15% (σ). These are much higher than the experimental values (15% and 10%, respectively), which suggests the H-bonding interaction in the SOR active site might have a significant effect on the S−Fe bond covalency. Indeed, in the H-bonding model, the calculated $\%S_{3p}$ character in these orbitals are 17% and 12%, in reasonable agreement with the experimental values.[62,63] The decrease in Fe−S bond covalency is mainly in the π bonding

(56) Loew, G. H.; Harris, D. L. *Chem. Rev.* **2000**, *100*, 407−419.
(57) Note that no calculations were performed on the H-bonded and α-carbon frozen models using the BP86 functional, as the H-bonding stabilizes the HS state by only 2 kcal/mol, which will be insufficient to change the 5 kcal/mol stable LS ground stage to a HS ground state.
(58) Szilagyi, R. K.; Metz, M.; Solomon, E. I. *J. Phys. Chem. A* **2002**, *106*, 2994.
(59) A fully optimized structure, i.e., no constraints, in B3LYP predicts that the low-spin ground state is 5 kcal/mol more stable than the high-spin ground state.
(60) Optimizations were attempted with only two constraints on the peptide fragment, but they caused less than 0.01 Å difference in geometry and less than 0.5 kcal/mol difference in the relative energies of the spin states.
(61) Pseudo-σ interaction implies that donor S_{3p} orbital is tilted off the Fe−S bond vector.

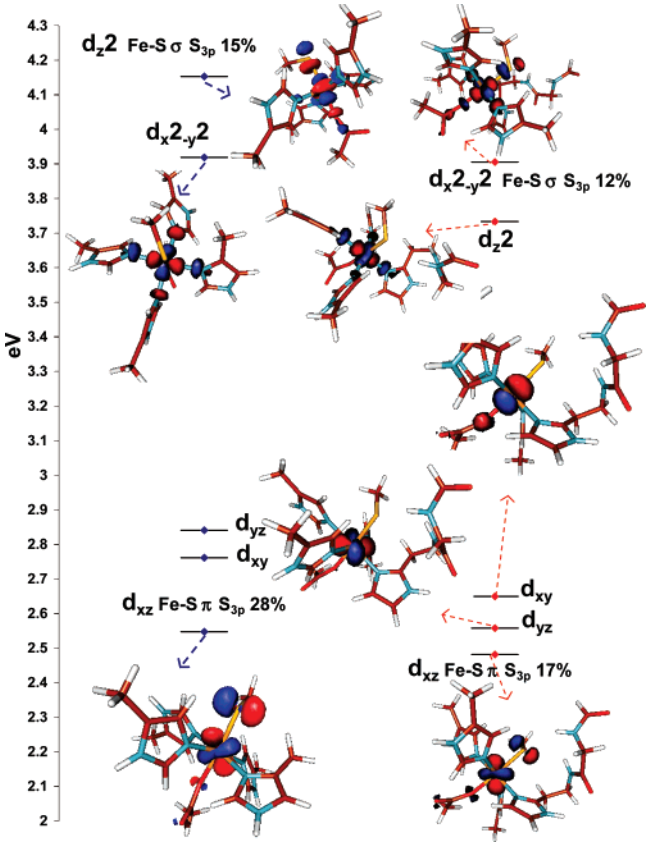

Figure 4. MO diagrams of the resting six-coordinate high-spin Fe^{III} active site without (left) and with (right) H-bonding interactions. The S_{3p} coefficients are indicated in text. Only the β contours are shown. The d_{yz} and d_{xy} contours of the model without H-bonding are not shown to avoid crowding.

orbital, consistent with the orientation of the H-bonds (Figure 3A). It is also worth noting that the total $\%S_{3p}$ values calculated using the BP86 method on the high-spin H-bonded model (Figure 3C) are ~39−40%, which are again much higher than the experimental value of 25% (15% π + 10% σ). This reflects the overestimation of Fe−S bonding by a pure functional and further indicates that B3LYP is better for describing the exchange in this system.

3. Low-Spin CN^- Adduct. The CN^- bound low-spin ferric active site was modeled with the α-carbon constraint that proved important to reproduce the correct ground state for the resting Fe^{III} site (Figure 3D). The geometry-optimized calculations on the CN^- bound form of model D indicate than the low-spin form is more stable by 90 kcal/mol, consistent with experiments. Thus, these α-carbon constraints were successful in reproducing the experimentally observed spin states of both the resting and the CN^- bound forms. Further, the H-bonds to the thiolate were included (model E), as they were crucial in reproducing the experimental covalency of the resting oxidized form.

A recent study by Clay et al., using vibrational spectroscopy and pulsed EPR techniques, has indicated the presence of at least three CN^- bound forms in solution: one linear and two bent conformations having Fe−C−N angles of 175°, 131°, and 125°, respectively.[20] From the ^2H_2O isotope effect observed on one set of C−N vibrations, it was proposed that the linear conformation is H-bonded to a solvent molecule.[20] Thus, in addition to the α-carbon constraints and H-bonding interactions that were necessary to reproduce the ground-state spin and Fe−S covalency of the HS model, an H-bond to the axial CN^- ligand from a H_2O molecule was also included in the LS model. Both the optimized geometries (E and E + H_2O, Table 2) have a linear Fe−CN unit and have shorter Fe−S and Fe−N bond lengths relative to the resting form, consistent with the low-spin state of the CN^- form. The optimized geometries with and without the H_2O H-bonded to the CN^- show that H-bonding leads to an elongation of the Fe−CN bond by 0.02 Å, which is compensated by 0.05 Å shortening of the Fe−S bond (Table 2, E and E + H_2O). This suggests that H-bonding to CN^- weakens the Fe−CN bond, which is compensated by strengthening of the trans Fe−S bond. These interactions determine the orientation of the single d-π hole in this low-spin Fe^{III} center (*vide infra*).

The MO diagrams of CN^- bound LS models E and E + H_2O (H-bonded to thiolate and H-bonded to thiolate and CN^-, Figure 5, left and right, respectively) show a normal low-spin t_2^5 configuration with one singly occupied β t_2 hole and two pairs (α + β) of unoccupied e orbitals (only three β orbitals shown in Figure 5). However, there is a very significant difference in their electronic structures. The t_2 hole of the low-spin Fe^{III} center is localized in the in-plane d_{xy} orbital in the H-bonded to thiolate model E, while it is in the d_{xz} (which is the Fe−S d-π antibonding) orbital in model E + H_2O. The description of model E is in contrast to the experimentally observed low-lying S → Fe CT, the low-energy t_2 pre-edge feature in the S K-edge XAS, and recently published ENDOR data, all of which indicate that the t_2 hole in the CN^- bound state is in the Fe−S d-π orbital.[20] The nature of the t_2 hole is determined by an interplay between the stabilization of the d_{xz}, d_{yz} orbitals by back-bonding to the CN π* orbitals and the destabilization of the d_{yz} orbital by the donation of the S_{3p} π orbital. In the case of the linear CN^- model with H-bonding to the thiolate (E), the back-bonding from the d_{xz}, d_{yz} orbitals along the Fe−CN axis into the two CN^- π* orbitals dominates, which results in localization of the t_2 hole on the d_{xy} orbital in the Fe−N_4 equatorial plane. H-bonding from the solvent molecule to the CN^- (Figure 5, E + H_2O) weakens this π backbonding interaction with one of the two d-π orbitals (evident from the decreased Fe_{3d} mixing in one of the two π* orbitals from 3.2% to 1%), and the t_2 hole is now localized in the antibonding Fe−S d-π d_{xz} orbital. Note that, of the two possible d-π orbitals along the Fe−CN bond, the Fe−S d-π orbital is higher in energy due to its π* nature, which localizes the t_2 hole in this orbital. Note that single-point calculations on bent Fe−CN models (as indicated by the Raman data) also show weakening of Fe−CN backbonding and similar

Table 2. Optimized Bond Distance (Å) and Angles (deg) of Linear, Bent, and H-Bonded CN^- Models Using B3LYP

	Fe–S	Fe–N_1	Fe–N_2	Fe–C	C–N	Fe–S–C	Fe–C–N	N–S	S---H–N
E	2.42	2.03	2.06	1.95	1.17	113.1	171.6	3.72, 3.97	126.5, 146.1
E + H_2O	2.37	2.03	2.06	1.97	1.17	115.3	174.6	3.74, 4.02	125.6, 145.9

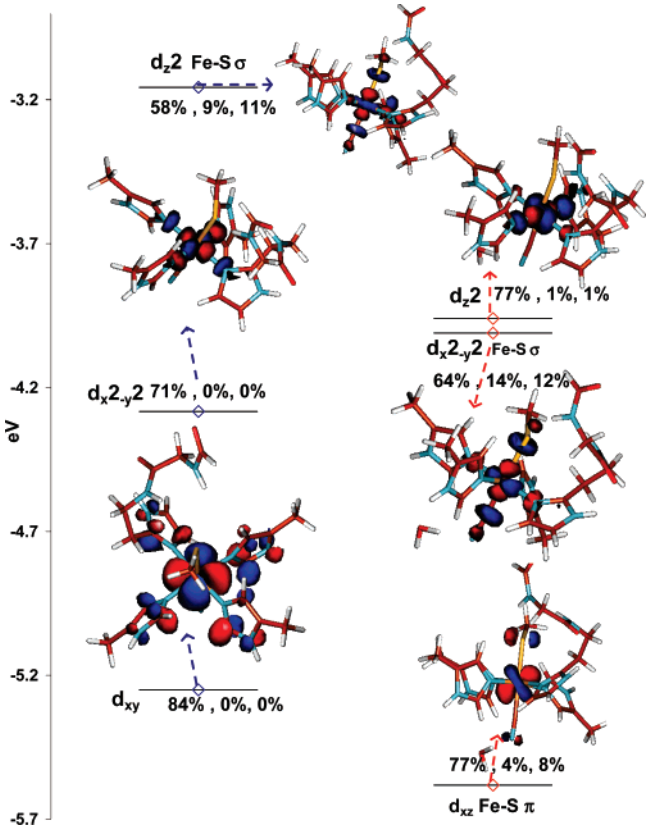

Figure 5. β contours of the E (left) and E + H_2O (right) models of the linear Fe−CN bound LS forms. The two α unoccupied contours are not shown for clarity. The designations of the orbitals are written next to them, and the $\%Fe_{3d}$, CN_{2p}, and S_{3p} are given as well.

localization of the t_2 hole in the d-π d_{xz} orbital (the effect of bending and H-bonding has an orientation dependence; Supporting Information, page S1).

A net result of these interactions is that the t_2 hole in the low-spin CN^- bound form has S_{3p} mixing, consistent with the low-energy pre-edge feature in S K-edge XAS and the presence of a CysS-dπ CT at 14 000 cm^{-1}.[10] The $\%S_{3p}$ mixing in the t_2 hole in the E + H_2O and the bent Fe−CN models is calculated to be 8% and 11%, respectively, lower than the experimentally observed 13% intensity in the 2469.5 eV feature in Figure 2. The total $\%S_{3p}$ in the unoccupied d orbitals is calculated to be 35% (11% d-π + 24% d-σ ($\alpha + \beta$)) for both the linear and bent models, which is distributed over one d-π and two d^{n+1} d-σ final states, as presented in section A. The experimental total $\%S_{3p}$ is estimated to be 33% (13% d-π and 20% d-σ).[64] Note that the Fe−S bond may be expected to get more covalent in its low-spin state relative to the high-spin state, but the very strong trans CN^- ligand in the low-spin state weakens it. This provides an explanation for the result that the S_{3p} coefficient in the d-σ orbital remains the same (12%) between the high-spin (Figures 4 and 5, right-hand sides) and the low-spin states. However, the total covalency of the Fe−S bond in the low-spin form is 35% (11% d-π + 2 × 12% d-σ), which is more than that of the high-spin form (25%) because the d-σ orbital is unoccupied in the low-spin state while it is half-occupied in the high-spin state. While this computational model provides a good qualitative description of the t_2 hole, the Fe−S d-π covalency is underestimated. Note that the nature of this t_2 hole is strongly dependent on the modeling of the CN^- fragment (as described above), and the estimation of the π Fe−S covalency may be improved by expanding the model. However, this is not essential for the properties investigated in the following sections.

The pre-edge of the resting Fe^{II} form could not be resolved due to its overlap with the rising edge. However, the geometric parameters of the calculated model (Fe−S, 2.35 Å; Fe−N, 2.20 Å) agree reasonably well with the published EXAFS data (Fe−S, 2.37 Å; Fe−N, 2.16 Å). The Fe−S bond covalency is calculated to be 14%, which is similar to the Fe−S bond covalency reported for an $Fe^{II}(SR)_4^{2-}$ model complex.[65]

Overall, the computational results indicate that the α-carbon constrained and H-bonded (to both thiolate and the trans axial ligand) model using the B3LYP hybrid functional reproduces the experimentally observed electronic and geometric parameters for the resting high-spin state and its conversion to the CN^- bound low-spin state. A different modeling approach was used in ref 17. Though neither the α-carbon constraints nor the H-bonding interactions were included, this model reproduced the high-spin resting state using the BP86 functional and a DN** basis set.[66] In another study, the BP86 functional with the 6-311g* basis set was used to describe the low-spin CN^- bound form.[67] Though this model gave the correct spin state and localization of the single t_2 hole, it predicted a low-spin ground state for the high-spin resting form and overestimated the Fe−S bond covalency in both high-spin and low-spin forms (which we find is significantly reduced upon inclusion of H-bonding and HF exchange in the computational models) that are both well reproduced by the model used here.

C. Reaction Mechanism. In this section, we use the experimentally calibrated computational model developed above to evaluate the reaction mechanism commonly invoked for SOR,[23] which involves reduction by one electron and double protonation of the superoxide anion to release H_2O_2. Figure 6 presents the results of the H-bonded thiolate model, which also includes H-bonding to the exchangeable axial ligand from a solvent H_2O molecule, i.e., the E + H_2O model in section B (the non-H-bonded model is given in the Supporting Information, Scheme S1). One intermediate (intermediate I), which has the characteristics of a ferric species, has been unambiguously reported in the literature by several groups.[13,23] The possible intermediates involved in the reaction mechanism were calculated in ref 17 using a non-H-bonded model, although the energies of individual steps were not evaluated and a low-spin Fe^{III}−OOH was assigned as intermediate I. Evaluating the energies of the individual steps of the mechanism and identifying

(62) Interestingly, the two *trans*-histidines, having short Fe−N_{His} bond lengths, form strong Fe−N σ bonds and define the unique (*z*) axis, while the $d_{x^2-y^2}$ orbital forms the σ bond with two other histidines and the axial ligands. This description is in good agreement with the results from Johnson et al. using EPR and VTVH MCD.[10]

(63) Note that a single-point calculation on the optimized H-bonded structure where the N−H's were substituted by −O−, i.e., amides were made esters, the Fe−S covalency was similar to that of the non-H-bonded model. This indicates that the reduction of Fe−S covalency is due to H-bonding.

(64) There is a large error bar (±3%) associated with this estimate due to the overlap of this higher energy feature with the rising edge transition.

(65) Kennepohl, P.; Solomon, E. I. *Inorg. Chem.* **2003**, *42*, 679−688.

(66) Only the dihedral angles between the histidine rings were constrained, which, reportedly, had no effect on the relative energies of the spin states of the structures examined.

(67) Yang, T.-C.; McNaughton, R. L.; Clay, M. D.; Jenney, F. E., Jr.; Krishnan, K.; Kurtz, D. M., Jr.; Adams, M. W. W.; Johnson, M. K.; Hoffman, B. M. *J. Am. Chem. Soc.* **2006**, *128*, 16566−16578.

(68) Noyes, R. M. *J. Am. Chem. Soc.* **1962**, *84*, 513−522.

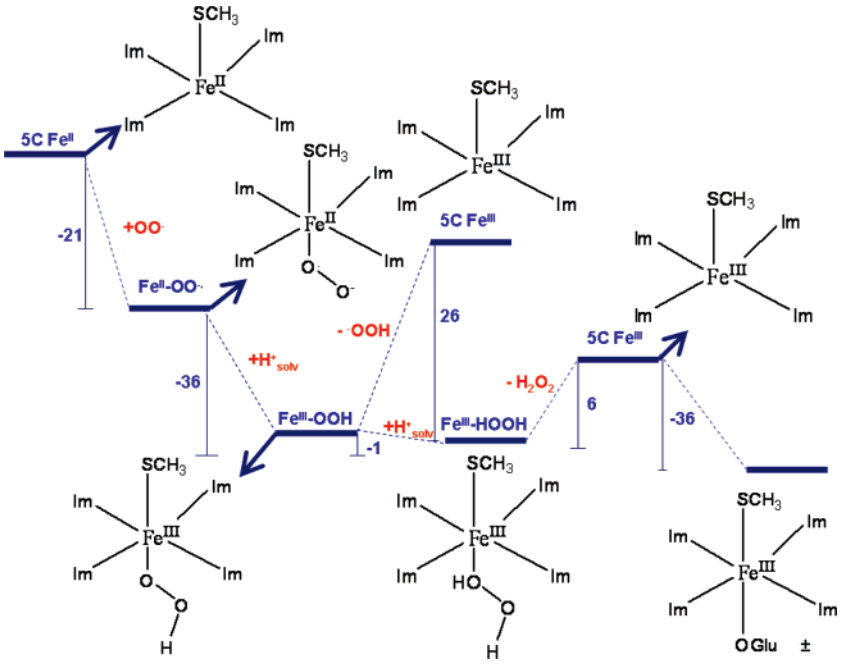

Figure 6. Reaction mechanism of SOR with H-bonding to the $CysS^-$ included. The numbers represent ΔE of individual steps ($\Delta E = E_{products} - E_{reactants}$); they were calculated using a PCM ($\epsilon = 4.0$) and are given in kcal/mol. Solvation energy of 260 kcal/mol was used for a proton (H^+_{solv}) in this scheme.[68] The computational model used for this calculation is described in Figure 3E. The H-bonds to thiolate and the axial ligand are not shown for clarity. $^{\pm}$In the E47A mutant, where the Glu is replaced by Ala, the axial ligand has been shown to be OH^- using rR.[72] The binding of a OH^- from water is calculated to be exothermic by −17 kcal/mol.

Table 3. Results of DFT Calculations on H-Bonded Models Relevant to the Mechanism

	spin	Fe–S (Å)	Fe–O (Å)	O–O (Å)	Fe–N (Å)	Fe–O–O (°)	S_S[a]	S_{Fe}[a]	S_O[a]	q_S[a]	q_{Fe}[a]
resting Fe^{II}	$S = 2$	2.35			2.21, 2.21		0.14	3.71		−0.66	1.36
Fe^{III} 5C	$S = {}^5/_2$	2.26			2.14, 2.13		0.53	4.08		−0.37	1.61
$Fe^{II}-O_2^-$	$S = {}^5/_2$	2.63	2.16	1.33	2.24, 2.18	123	0.03	3.78	0.5, 0.5	−0.79	1.54
$Fe^{III}-OOH$	$S = {}^5/_2$	2.45	1.95	1.44	2.19, 2.17	123	0.24	4.15	0.27	−0.59	1.73
$Fe^{III}-OOH$	$S = {}^1/_2$	2.41	1.81	1.45	2.07, 2.00	118	−0.05	0.99	0.11	−0.50	1.47
$Fe^{III}-H_2O_2$	$S = {}^5/_2$	2.29	2.75	1.45	2.15, 2.15	125	0.53	4.10		−0.38	1.71
resting Fe^{III}	$S = {}^5/_2$	2.43	1.95		2.2, 2.16		0.31	4.19		−0.53	1.76

[a] Mulliken spin densities and charges.

possible intermediates (including spin states) will be the main focus of this section. The relevant geometric and ground-state parameters are listed in Table 3.

The first step involves attack by the superoxide anion at the open coordination position of the resting Fe^{II} to form an inner-sphere complex. The ΔE of the reaction is −21 kcal/mol. This species is best described as an $Fe^{II}-$superoxide complex, as the O−O distance is 1.33 Å and the spin density on the O_2 fragment is 1.0. Thus, it is important to note that this step does not involve electron transfer from the Fe^{II} center to the bound superoxide ion, and hence this species is not likely to be the experimental intermediate I, which has spectroscopic characteristics of an Fe^{III} species.[13,23]

The next step involves protonation of the bound superoxide to generate an η^1-HOO−Fe complex.[69] This species is best described as an $Fe^{III}-OOH$ species on the basis of the optimized Fe−O, O−O bond distances and the resultant spin densities on Fe and OOH (Table 3). The calculated energies of the geometry-optimized high-spin and the low-spin states of this model indicate that the former is more stable by 4 kcal/mol. This is in contrast to the results in ref 17, where a low-spin ground state was calculated to be more stable. Thus, this computational model, which predicts the correct ground state and thiolate covalency of both the resting high-spin and the CN^- bound low-spin forms of SOR, predicts a high-spin ground state of an $Fe^{III}-OOH$ intermediate. The high energy of this protonation step, −35 kcal/mol (using 260 kcal/mol for solvated H^+), will help overcome any barrier that may be involved in protonating the distal oxygen of this solvent-exposed $Fe^{II}-O_2^-$ adduct. The H^+ may be donated by Lys48 or abstracted from bulk solvent, as this site is very solvent exposed. Thus, the above results favor a high-spin $Fe^{III}-OOH$ as the first stable ferric species formed in the reaction cycle. Note that the large driving force for the formation of this species is consistent with its diffusion-controlled rate of formation. Further, the favorable protonation energy will help drive the process and explain the lack of a ^2H isotope effect in its formation.[14]

At this point, heterolytic cleavage of the Fe−O bond to generate a five-coordinate high-spin Fe^{III} center and an −OOH

(69) This is consistent with a recent report of an end-on bound Fe−OO intermediate trapped crystallographically in the E114A mutant. Katona, G.; Carpentier, P.; Nivière, V.; Amara, P.; Adam, V.; Ohana, J.; Tsanov, N.; Bourgeois1, D. *Science* **2007**, *316*, 449.

ion may be possible. In fact, a potential energy scan of Fe−O bond in the non-H-bonded model of this active site results in a heterolytic Fe−O cleavage (with a barrier of +26 kcal/mol), in contrast to homolytic Fe−O cleavage generating Fe^{II} and an $^{\bullet}OOH$ radical as found in DFT calculations of high-spin non-heme iron hydroperoxide intermediates with neutral ligands.[70] However, this step is calculated to be endothermic (for the computational model used here) and will introduce a 26 kcal/mol energy barrier (ΔE) in the reaction pathway. An alternative energetically favored path involves protonation of the proximal oxygen of the $Fe^{III}-OOH$ species, resulting in an $Fe^{III}-O_2H_2$ species. This process is enthalpically favorable ($\Delta E = -1$ kcal/mol, using a solvated proton), as the resulting high-spin $Fe^{III}-O_2H_2$ species is stabilized by strong interaction with the axial H-bonded thiolate (the Fe−S bond shortens from 2.45 Å in $Fe^{III}-OOH$ to 2.29 Å in $Fe^{III}-O_2H_2$; Table 3). Note that the favorable enthalpy of protonation does not reflect a greater stability of the $Fe^{III}-O_2H_2$ species relative to the $Fe^{III}-OOH$ species (see calculated ΔG's below). The ΔE for this step is +6.6 kcal/mol for a model that does not include the H-bonding interaction with the exchangeable axial ligand from the solvent molecule. This interaction had to be included in the model to get reasonable agreement with the S K-edge XAS data on the low-spin CN^- bound form and is observed in the crystal structure of this $Fe^{III}-OOH$ species. This additional interaction from a solvent molecule makes the reaction more favorable by ~8 kcal/mol (6.6 kcal/mol + 1 kcal/mol from Figure 6) by stabilizing the weakly bound H_2O_2 by H-bonding. The resulting $Fe-O_2H_2$ species has a long Fe−O bond (2.7 Å), which facilitates the release of the final H_2O_2 product. Thus, the anionic thiolate ligand weakens the Fe−OOH bond, favoring its protonation and cleavage. Note that, in compound 0 of peroxidases, the protonation of a proximal oxygen of an $Fe^{III}-OOH$ species is calculated to have a barrier of 9 kcal/mol (including ZPE correction).[71] However, this is still less than the $\Delta G^{\ddagger}$ of diffusion of a small ion in solution (11−12 kcal/mol) involved in the formation of the $Fe^{II}-O_2^-$ adduct. The following step is cleavage of the weak $Fe-(O_2H_2)$ bond, which is endothermic by only $\Delta E = 8$ kcal/mol, and this process is associated with a further 0.03 Å decrease in the Fe−S bond length. The small dissociation energy of the H_2O_2 implies that the axial thiolate also helps avoid product inhibition. It is also possible that the axial glutamate residue displaces this weakly bound H_2O_2, as its binding is exothermic by −36 kcal/mol. In the E47A mutant, the Glu is replaced by a H_2O, which binds as HO^- from rR studies[72] and is also calculated to be exothermic by −17 kcal/mol. This results in the formation of the 6C Fe^{III} resting form of the enzyme, which would be re-reduced in turnover. Note that the presence of the axial glutamate residue competes with superoxide binding to the Fe^{III} site and has been proposed to be an important factor in avoiding superoxide dismutase activity (*vide infra*).[2]

Along the calculated reaction pathway, three species could be identified as possible candidates for the observed intermediate I, namely the $Fe^{II}-O_2^-$, the $Fe^{III}-OOH$, and the $Fe^{III}-O_2H_2$ species. Though the calculated ΔE's provide some insight into the favored pathway, the ΔG's are more useful in evaluating the feasibility of a possible intermediate. The ΔG for the formation of the $Fe^{III}-OOH$ upon protonation of the $Fe^{II}-O_2^-$ is calculated to be −25 kcal/mol. The large driving force for protonation, along with the observation that the deprotonated species is Fe^{II} in nature, disfavors the $Fe^{II}-O_2^-$ species as the ferric intermediate I. The heterolytic dissociation of the Fe−OOH to Fe^{III} and HOO^- has a ΔG of +14 kcal/mol that will result in an estimated rate constant of 400 s^{-1} (using the Eyring equation and assuming $\Delta G^{\ddagger} = \Delta G$ for an endothermic process without any additional barrier), which is significantly lower than the experimentally observed rate. Thus, this step cannot be involved in the reaction pathway. Alternatively, the protonation of this $Fe^{III}-OOH$ species has a ΔG of +5.4 kcal/mol, and the further dissociation of the $Fe-O_2H_2$ species has a ΔG of −10 kcal/mol. The lack of a significant barrier ($\Delta G^{\ddagger} = 9$ kcal/mol)[71] and requirement of a H^+ for decay of the $Fe^{III}-OOH$ are consistent with the pH-dependent diffusion-controlled decay of intermediate I.[73] Also, the observed intermediate has a S → Fe CT band that is blue-shifted to 600 nm from 647 nm in the resting enzyme.[14,15] This blue shift of the S → Fe CT is indicative of a stronger ligand field around the Fe^{III} in the intermediate which is only present in the $Fe^{III}-OOH$ species.[74] Thus, the high-spin $Fe^{III}-OOH$ species is the likely candidate for intermediate I.

Table 4. Optimized Fe−O Bond Lengths and Calculated $Fe^{III}-OOH$ Protonation Enthalpies

model	Fe–O (Å)	ΔE (kcal/mol)
$(MeS)Fe^{III}(His)_4OOH$ H-bonded	1.95	+6.7
$(F)Fe^{III}(His)_4OOH$	1.95	+14.1
$(H_2O)Fe^{III}(His)_4OOH$	1.89	+43.0
$(MeS)Fe^{III}(His)_4OOH$	1.95	+2.5

The above mechanism is in general agreement with the mechanisms proposed by Kurtz et al. and Nivière et al. but with some differences.[14,15] While Nivière et al. suggested that the intermediate I is a high-spin side-on Fe^{III} deprotonated peroxide, our results here suggest that the deprotonated $Fe-O_2$ adduct is Fe^{II} superoxide in nature. In the DFT calculations, a side-on $Fe^{III}-\mu_2-O_2$ species is formed only in the absence of H-bonding to the thiolate (Supporting Information, Scheme S1). On the basis of DFT-calculated energies, Kurtz et al. favor a low-spin $Fe^{III}-OOH$ as intermediate I,[17] but we find the high-spin $Fe^{III}-OOH$ species to be more stable by 4 kcal/mol. Also, protonation of a low-spin $Fe^{III}-OOH$ will result in the formation of a high-spin $Fe^{III}-O_2H_2$ species and will involve a spin-crossing, which will have a barrier. The possibility of a second intermediate has also been proposed by Nivière et al. At this point, the calculated mechanism shown in Figure 6 does not provide sufficient support for the presence of another intermediate.

D. Perturbations to the Model: Contributions to Reactivity. The presence of a H-bonded thiolate ligand is a unique feature of the SOR active site. The following sections address the effect of the axial ligand on the two key reaction steps: the protonation of the $Fe^{III}-OOH$ species and the reduction of the

(70) Lehnert, N.; Ho, Y. N. R.; Que, Jr. L.; Solomon, E. I. *J. Am. Chem. Soc.* **2001**, *138*, 12802−12816.
(71) Derat, E.; Shaik, S. *J. Phys. Chem. B* **2006**, *110*, 10526−10533.
(72) Mathe, C.; Nivière, V.; Mattioli, T. A. *J. Am. Chem. Soc.* **2005**, *127*, 16436−16441.
(73) Note that another ^{2}H-sensitive decay pathway of the intermediate I has been proposed by Kurtz et al. which has a much slower rate (50 s^{-1}). The possible candidate for this pathway could be protonation of the proximal oxygen from a nearby ionizable residue or a H_2O molecule.[14]
(74) The S π and Fe d-π CT energy gap is calculated to be blue-shifted by 1500 cm^{-1}, consistent with this proposal.

Table 5. Calculated Shift of the Reduction Potential upon Axial Ligand Perturbation

model	ΔIE (mV)
$(MeS)Fe^{III}(His)_4Glu$	+137
$(MeS)Fe^{III}(His)_4Glu$ H-bonded	0
$(F)Fe^{III}(His)_4Glu$	−516
$(H_2O)Fe^{III}(His)_4Glu$	+3000

ferric site generated at the end of the reaction in Figure 6 for further turnover. The following perturbations will be computationally evaluated: the effect of the axial ligand (H-bonded MeS^- to H_2O and F^-) and the effect of H-bonding (H-bonded MeS^- to MeS^-). These calculations use a model that includes only H-bonding to the thiolate and not to the exchangeable axial ligand, i.e., model E in Figure 3.

1. Protonation of Fe^{III}−OOH. The calculated Fe−O bond length and the energy required to protonate the proximal oxygen of the Fe^{III}−OOH species for the different models listed above are given in Table 4. Replacing the negatively charged thiolate with a neutral H_2O results in a shorter optimized Fe−O bond length (1.89 Å with H_2O vs 1.95 Å with a thiolate). The stronger Fe−OOH bond with the trans H_2O ligand makes the subsequent protonation of this species to form H_2O_2 energetically uphill by 43 kcal/mol (also, the heterolytic cleavage into 5C Fe^{III} and $^-$OOH fragments is calculated to be uphill by >100 kcal/mol). This is in agreement with the lack of Fe−O bond heterolysis in the 6C high-spin Fe^{III}−OO^{t}Bu complex with neutral ligands and facile Fe−O heterolysis observed in the 6C high-spin Fe^{III}−OOH species with an anionic ligand.[24,70] Interestingly, substitution of the axial ligand with another anionic ligand like F^- results in a 7 kcal/mol unfavorable protonation energy relative to that of a trans thiolate ligand. This suggests that, although the anionic nature of the thiolate ligand plays a dominant role in lowering the protonation energy (by 29 kcal/mol) relative to that induced by a neutral ligand, its covalent nature further assists the protonation by 7 kcal/mol. H-bonding to the thiolate makes it a weaker donor and results in a process that is 4.2 kcal/mol more endothermic relative to that observed with a non-H-bonded thiolate.

2. Redox Potential. The SOR active site has a redox potential of ∼250−300 mV. This process involves a 6C ferric species and a 5C ferrous species (i.e., Fe^{III}−Glu + e^- → Fe^{II} + Glu^-) and is essential for the re-reduction of the Fe^{III} during turnover.

The effects of the above perturbations of the axial thiolate ligand on the energy of this redox process are tabulated in Table 5. Note that these are shifts in ionization energies (IE) calculated using a PCM and not reduction potentials. However, these shifts in IE are reasonable approximations for the shifts in reduction potentials, as the contributions from entropy, zero-point energy, and solvation of the axial ligand should be similar between these models. Changing the axial thiolate to a neutral H_2O shifts the redox potential by more than +3 V. This is expected, as this substitution changes the charge of the model. On substituting the thiolate with an F^-, the potential shifts more negative by 516 mV, which could imply greater stabilization of the Fe^{III} state by F^- or a greater stabilization of the Fe^{II} state by the $CysS^-$ ligand. Note that the SOR redox couple includes an increase in coordination number upon oxidation. Thus, the oxidation process can be divided into two steps: oxidation of a reduced 5C site and subsequent coordination of the glutamate ligand to the oxidized 5C site. The calculations on a 5C site show that replacing the $CysS^-$ with F^- shifts this reduction potential only by +44 mV, indicating that this ligand change has a negligible effect on the relative stabilities of the 5C Fe^{II} and the 5C Fe^{III} states. However, the F^- donates less charge to the Fe and increases its Lewis acidity. This results in an increased sixth ligand binding energy (∼13 kcal/mol = ∼560 mV) for the F^- bound oxidized site. Thus, F^- binding results in additional stabilization of the 6C Fe^{III} state, which shifts the reduction potential of the coupled redox process by −516 mV. The H-bonded thiolate has a redox potential shifted by −137 mV relative to that of a non-H-bonded thiolate ligand. This is in contrast to the results of several past studies, where H-bonding has been found to shift the redox potential more "positive" as it stabilizes the increased charge density in the reduced form.[36] H-bonding affects differently the oxidation of a reduced 5C site and the subsequent coordination of the glutamate ligand to the oxidized 5C site. The calculations on a 5C site show that the H-bonding interaction with the thiolate shifts the reduction potential by +250 mV, as observed in past studies.[36] However, the H-bonded thiolate donates less charge to the Fe and increases its Lewis acidity. This results in an increased sixth ligand binding energy (∼9 kcal/mol = ∼387 mV) for the H-bonded oxidized site. The net result is that H-bonding shifts the coupled redox process by −137 mV.

In summary, the anionic nature of the thiolate ligand is necessary to raise the pK_a of Fe^{III}−OOH species while keeping its E_o (tuned by the H-bond to the cysteine) in the range required for SOR reduction. The covalent character of the thiolate−Fe bond helps to further weaken the Fe−OOH bond by +7.4 kcal/mol relative to the effect of a noncovalent anionic ligand like F^-. This decrease in protonation affinity due to a covalent thiolate corresponds to a ∼5 log unit increase in the pK_a of the Fe^{III}−OOH species.

E. SOR vs SOD. Interestingly, the SOR active site shows very limited SOD activity (0.5−1% of native Fe-type SODs), despite having a redox potential (+250 mV) comparable to that of the Fe−SOD active site, which is in between those of the $O_2^- \rightarrow O_2 + e^-$ and $O_2^- + 2H^+ + e^- \rightarrow H_2O_2$ couples.[75] DFT calculations were employed to investigate the oxidation of superoxide by the H-bonded SOR in comparison to a model of the Fe−SOD active site (Figure 7).[76] Elaborate spectroscopic characterization and DFT calculations of Fe−SOD have been reported, where the importance of the second-sphere residues has been demonstrated.[77,78] We employ a simpler model here, consisting of three imidazoles, one acetate, and one hydroxide/water, and focus mainly on the energies for the individual steps (which are not evaluated elsewhere) as a reference for the SOD activity of the SOR active site. Inner-sphere superoxide binding to Fe^{III} was assumed. The relevant bond lengths and spin densities are given in Table 6. The superoxide binding is exothermic for both the SOR and SOD sites, leading to the formation of an Fe^{III}−OO^- complex. The binding energy is higher for the SOR (−57 kcal/mol) than for the SOD (−29 kcal/mol) active site. This is largely the result of the two anionic

(75) Jovanović, T.; Ascenso, C.; Hazlett, K. R. O.; Sikkink, R.; Krebs, C.; Litwiller, R.; Benson, L. M.; Moura, I.; Moura, J. J. G.; Radolf, J. D.; Huynh, B. H.; Naylor, S.; Rusnak, F. *J. Biol. Chem.* **2000**, *275*, 28439−28448.
(76) Cooper, J. B.; McIntyre, K.; Badasso, M. O.; Wood, S. P.; Zhang, Y.; Garbe, T. R.; Young, D. *J. Mol. Biol.* **1995**, *246*, 531−544.
(77) Jackson, T. A.; Brunold, T. C. *Acc. Chem. Res.* **2004**, *37*, 461−470.
(78) Han, W.-G., Lovell, T.; Noodleman, L. *Inorg. Chem.* **2002**, *41*, 205−218.

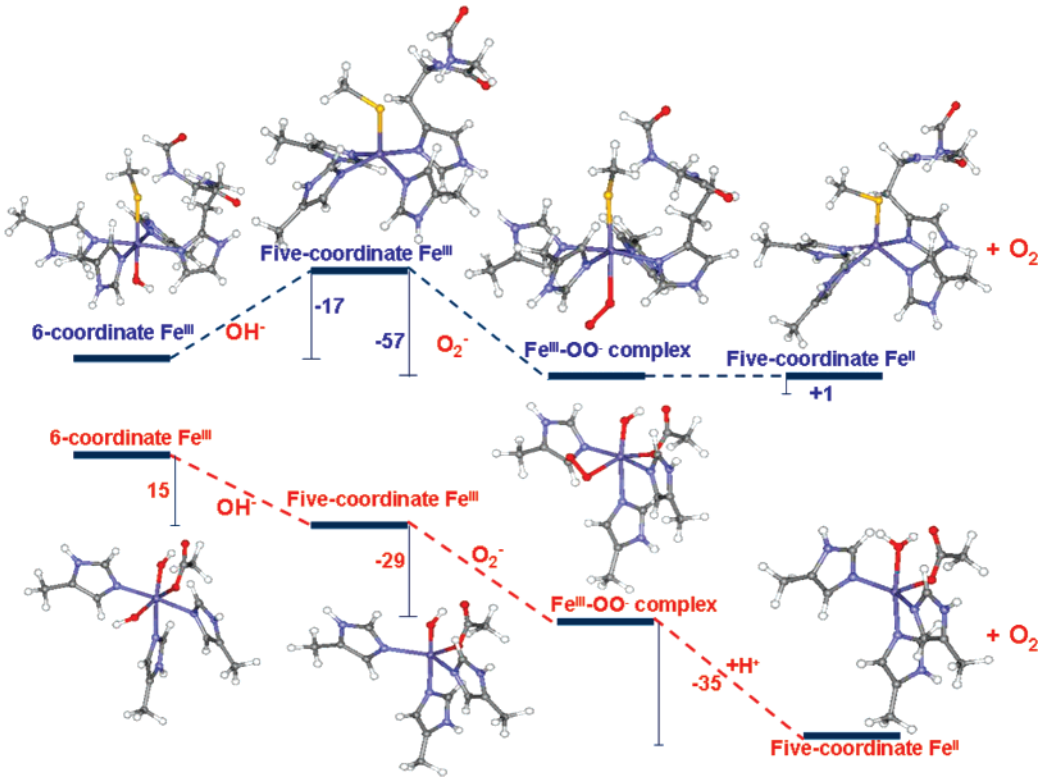

Figure 7. Comparison of energies of superoxide oxidation by SOR (upper panel) and SOD (lower panel) active sites (energies (ΔE), calculated using a PCM ($\epsilon = 4.0$) and given in kcal/mol). Solvation energy of 260 kcal/mol was used for an H^+.

Table 6. Relevant Bond Lengths and Mulliken Spin Densities for Species Involved in SOD Cycle

model		Fe–L_{trans}[a]	Fe–O[a]	O–O[a]	$spin_{Fe}$	$spin_{O-O}$
5C Fe^{III}	SOR	2.26			4.08	
	SOD	1.90			4.20	
$Fe^{III}+O_2^-$	SOR	2.43	2.24	1.28	4.03	1.51
	SOD	2.05	2.09	1.30	4.15	1.28
Fe^{II}	SOR	2.35			3.71	
	SOD	2.07			3.79	
$Fe^{III}-OH$	SOR	2.47	1.89		4.21	
	SOD	2.06	1.88		4.24	

[a] In angstroms.

donors present at the SOD active site ($^-$OH and CH_3COO^-), which makes a third anionic ligand binding less favorable relative to the one anionic donor in SOR ($^-$SMe). The higher shift of electron density from O_2^- to Fe^{III} in SOR leads to an $Fe^{II}-O_2$-like species having a O–O bond length of 1.28 Å and a spin density of 1.5 on the O_2 fragment (Table 6). Thus, facile O_2 dissociation is calculated for this species, which is only 1 kcal/mol uphill. Note that this represents the ΔE for the process. The ΔG will be ~12 kcal/mol downhill, as this step involves O_2 dissociation. In SOD, this step is H^+-driven (as $Fe^{III}-OH$ is converted to $Fe^{II}-OH_2$ in the product) and very exothermic (−35 kcal/mol).[79] It is important to note that these results indicate that a five-coordinate SOR active site *is capable of SOD activity*.

However, while the resting ferric SOD active site is five-coordinate, resting SOR is six-coordinate, and the reaction with O_2^- would require dissociation of the axial glutamate ligand. This dissociation energy (ΔE) for the glutamate residue in the resting SOR active site is calculated to be +36 kcal/mol. Although a 5C active site is generated during turnover (Figure 6), one also needs to consider the possibility of H_2O binding to form an $Fe^{III}-OH$ species, which is kinetically favored over reaction with superoxide ($[O_2^-] = 10^{-6}-10^{-9}$ M under turnover conditions), as proposed by Kurtz et al.[23] From Figure 7, the ΔE for $Fe^{III} + 2H_2O \rightarrow Fe^{III}-OH + H_3O^+$ for the open five-coordinate Fe^{III} active site in SOR is favorable by −17 kcal/mol. In contrast, this process is uphill, $\Delta E = +15$ kcal/mol, for the five-coordinate Fe^{III} site in SOD. This is consistent with the SOD active site remaining five-coordinate in solution,[80] while the E47A mutant of SOR (this mutant lacks the axial carboxylate ligand) has a bound $^-$OH at physiological pH.[72] Thus, for SOR but not SOD, O_2^- binding to the Fe^{III} site requires dissociation of an anionic ligand, which is endothermic by at least ~15 kcal/mol (for OH^-; 36 kcal/mol for Glu), along the reaction coordinate (Figure 7, left). This will effectively inhibit the SOD activity of the SOR active site.

Discussion

The resting high-spin Fe^{III} site of SOR has an axial Fe–SCys bond with two peptide NH–S H-bonding interactions. Its S K-edge XAS exhibits a large t_2–e splitting (1.2 eV), such that the σ and π covalency of this cysteine thiolate–Fe^{III} can be directly measured (Figure 2). The $\%S_{3p}$ characters (i.e., covalency) in the t_2 and e Fe_{3d} orbitals are obtained experimentally to be 15% and 10%, respectively (total 25%). The total Fe–S bond covalency of SOR is comparable to that of H-bonded heme thiolate models (30%).[36] Comparison of the H-bonded thiolate ligand with a neutral (H_2O) and an anionic ligand (F^-) reveals

(79) Lah, M. S.; Dixon, M. M.; Pattridge, K. A.; Stallings, W. C.; Fee, J. A.; Ludwig, M. L. *Biochemistry* **1995**, *34*, 1646–1660.

(80) Tierney, D. L.; Fee, J. A.; Ludwig, M. L.; Penner-Hahn, J. E. *Biochemistry* **1995**, *34*, 1661–1668.

that the thiolate plays the role of a covalent anionic ligand. The anionic character of the thiolate ligand increases the pK_a of the $Fe^{III}-OOH$ intermediate, facilitating its protonation by 29 kcal/mol and tuning its potential down to a physiological range. The covalent character of the thiolate facilitates the reaction by further lowering the protonation energy of the high-spin $Fe^{III}-OOH$ intermediate by 7.5 kcal/mol relative to that of a noncovalent anionic donor like F^-. The high π covalency of the resting ferric SOR site can also facilitate electron transfer into the active site by providing efficient ligand superexchange coupling into the protein.[81]

The mechanism of superoxide reduction by SOR has been found to involve one or more intermediates.[23,16] One is proposed to be a high-spin side-on peroxide on the basis of resonance Raman studies.[22] We could computationally stabilize a side-on η^2-$Fe^{III}-$peroxo species only in the absence of H-bonding to the thiolate, and its protonation (leading to an $Fe^{III}-OOH$ species) was energetically very favorable (Supporting Information, Scheme S1). On including the conserved H-bonding residues to the thiolate ligand, which are necessary to reproduce the experimental Fe−S bond covalency, a peroxide level intermediate could be generated only upon protonation. This high-spin $Fe^{III}-OOH$ species is consistent with the experimentally observed stronger ligand field in the intermediate ($S \rightarrow Fe^{III}$ CT blue-shifted by $\sim$1100 cm^{-1}) relative to that in the resting ground state (HOO^- is a stronger donor ligand that $GluO^-$). The formation of this O_2^- adduct and its further protonation, with a large driving force (which helps overcome barriers), and the decay requiring a H^+ (with $\Delta G^{\ddagger} = 9$ kcal/mol) are consistent with the diffusion-controlled pH-independent rate of formation and diffusion-controlled pH-dependent rate of decay observed experimentally.[14] The above mechanism is consistent with recent results from Kitagawa et al., who identified a high-spin $Fe^{III}-OOH$ species as an intermediate in a functional model of SOR.[24] It is important to note that, with a noncovalent anionic axial ligand like F^- in place of the thiolate, this step is +14 kcal/mol uphill, which would be detrimental toward the fast kinetics required for this enzyme.

The active site of SOR is similar to the active site of cytochrome P450, which also has an axial cysteine coordination and an equatorial N_4 coordination. However, the porphyrinato dianion in the active site of P450 provides a strong equatorial ligand field and an aromatic macrocycle with an additional 2− charge.[23] This produces dramatic differences in the reactivities of the $Fe^{III}-OOH$ intermediate involved in both active sites. The additional negative charge makes the protonation of the $Fe^{III}-OOH$ (compound 0) species in P450 is more favorable than protonation of SOR. Protonation of the distal oxygen of compound 0 in P450 leads to an energetically favorable O−O bond heterolysis ($\Delta E = -40$ kcal/mol), forming compound I, where the Fe^{III} gets oxidized to Fe^{IV} and the porphyrin ring gets oxidized to a ligand radical. An analogous O−O bond heterolysis of the $Fe^{III}-OOH$ species in the SOR active site results in an Fe^{IV} and histidine cation radical species and is calculated to be $\sim$+250 kcal/mol uphill in energy, clearly demonstrating the necessity of the porphyrin dianion in stabilizing the $Fe^{IV}-$oxo ligand radical species. Protonation of the proximal oxygen in compound 0 in P450 leads to the formation of an $Fe^{III}-O_2H_2$ species analogous to SOR. However, due to the strong equatorial ligand field of the porphyrin ring, compound 0 in P450 is low-spin. Thus, protonation and elimination of H_2O_2 from the low-spin compound 0, which will form the 5C high-spin Fe^{III} state, will involve a barrier associated with the forbidden two-electron spin flip. Indeed, the elimination of H_2O_2 in the P450 active site is experimentally determined to be <1%.[82,83] However, the high-spin nature of the $Fe^{III}-OOH$ intermediate in SOR enables facile H_2O_2 release, forming a high-spin product.

An important feature of the SOR active site is the presence of the H-bonded thiolate in the first coordination sphere of Fe trans to the O_2^- binding site. The H-bonding to the active site causes a significant decrease of the Fe−S bond covalency (decrease in covalency of 11% π and 3% σ in model D, Figure 3), which shifts the reduction potential by −137 mV. This negative shift in $E°$ is opposite to the results in previous studies, where positive shifts are observed upon H-bonding. It reflects the net effect of two opposing factors: (a) increased stabilization of the 5C Fe^{II} site (+250 mV, consistent with previous results)[36] and (b) increased sixth axial ligand binding affinity (due to increased Lewis acidity) of the 5C Fe^{III} site (−387 mV). A further effect of the H-bonding to the thiolate is in the nature of the $Fe^{II} + O_2^-$ adduct. It can be described as an η^1-O_2^-−Fe^{II} species in the presence and an η^2-O_2^{2-}−Fe^{III} species in the absence of H-bonding. The $Fe^{II}-\eta^1$-O_2^- species has higher net charge on the distal oxygen and a higher energy HOMO donor orbital that activates it for protonation relative to an $Fe^{III}-\eta^2$-O_2^{2-} species, where the charge on the peroxide moiety is reduced because of its very covalent charge donation to the Fe^{III}.[84]

Finally the five-coordinate SOR active site is calculated to be *able to perform superoxide oxidation to dioxygen*. The lack of SOD activity in SOR enzymes then appears to result from a favorable sixth ligand binding energy of the solvent-exposed SOR active site, as has been proposed previously by Kurtz et al.[23] The Lewis acidity of the SOR active site, having only one anionic ligand, is such that the Fe^{III} state generated during turnover binds a glutamate ligand or an −OH ligand. Superoxide binding to the 6C Fe^{III} SOR site would entail a dissociative mechanism that is calculated to be endothermic by at least $\sim$15 kcal/mol, which will preclude SOD activity. In contrast, the Fe−SOD active site, which has two strong anionic ligands (hydroxide and aspartate), has an unfavorable energy for binding an additional anionic −OH ligand and thus remains five-coordinate at physiological pH's, allowing facile SOD activity.

Acknowledgment. This research was supported by NIH Grants GM 40392 and NSF-CHE 446304 (E.I.S.), RR-01209 (K.O.H.), GM 60329 (M.W.W.A. and M.K.J). A.D. has an Evelyn Laing McBain fellowship from Stanford University. A.D. acknowledges Dr. M. D. Clay, Dr. Andrea Decker, and Dr. Diego Del Rio for valuable discussions. SSRL operations

(81) Solomon, E. I. *Inorg. Chem.* **2006**, *45*, 8012−8025.

(82) Martinis, S. A.; Atkins, W. M.; Stayton, P. S.; Sligar, S. G. *J. Am. Chem. Soc.* **1989**, *111*, 9253−9254.

(83) In addition to this barrier due to a spin state change, a low-spin $Fe^{III}-$OOH species has a very covalent Fe−O bond, which is calculated to make protonation uphill by 35 kcal/mol in the SOR active site.

(84) The μ^1-O_2^-−Fe^{II} species has higher charge (-0.53) on the distal oxygen and a filled occupied π^*_v orbital at −3.9 eV having 40% distal O_{2p} coefficient relative to the μ^2-O_2^{2-}−Fe^{III}, which has a net total charge of (-0.37) and an orbital at −4.2 eV with 36% O_{2p} character.

are supported by the U.S. Department of Energy, Office of Basic Energy Sciences. The SSRL Structural Molecular Biology Program is supported by the National Institutes of Health, National Center for Research Resources, Biomedical Technology Program, and by the Department of Energy, Office of Biological and Environmental Research.

Supporting Information Available: All optimized geometries, MO diagram of the H-bonded CN^- bound form and the reaction scheme without H-bonding, and complete ref 42. This material is available free of charge via the Internet at http://pubs.acs.org.

JA064167P